


# SCIENTIFIC REPORTS

OPEN

## Precipitates and Particles Coarsening of 9Cr–1.7W–0.4Mo–Co Ferritic Heat-Resistant Steel after Isothermal Aging

Qiuzhi Gao<sup>1</sup>, Yanan Zhang<sup>2</sup>, Hailian Zhang<sup>3</sup>, Huijun Li<sup>4</sup>, Fu Qu<sup>1</sup>, Jian Han<sup>4</sup>, Cheng Lu<sup>4</sup>, Bintao Wu<sup>4</sup>, Yao Lu<sup>4</sup> & Yan Ma<sup>4</sup> 

The precipitates obtained by EPE technology from the 9Cr-1.7W-0.4Mo-Co ferritic heat-resistant steel subject to isothermal aging were investigated using SEM, TEM and XRD. The particle size distribution and the coarsening kinetics of  $M_{23}C_6$  with duration of isothermal aging were also analyzed with or without consideration of Laves phase. The results show that the isolated dislocations were detected in delta ferrite interior, and the precipitates on delta ferrite and martensite boundaries are obviously larger than other locations.  $Fe_2W$ -Laves phase can only be found as duration of aging time to 2000 h, and is preferential to form adjacent to  $M_{23}C_6$  particles. The small  $M_{23}C_6$  particles firstly coarsen, but the large  $M_{23}C_6$  are relatively stable during short aging. The total coarsening rate of  $M_{23}C_6$  precipitates is  $9.75 \times 10^{-28} m^3 s^{-1}$ , and the coarsening of  $M_{23}C_6$  depends on the formation of Laves phase.

9~12wt.% Cr ferritic creep steels, as the key materials increasing the thermal efficiency of steam power plants, are widely used in power industries due to its excellent high temperature stability, high creep strength and stress corrosion cracking<sup>1–4</sup>. The excellent properties have been achieved through apparently minor compositional changes to well established steels like P91, P92 and P122<sup>5,6</sup>. However, the main problem of 9~12 wt.% Cr ferritic steels that has been addressed is that their microstructural instability with a degradation in oxidation resistance during long term service at temperature up to 923 K<sup>7</sup>. New alloys, such as NF12 and SAVE12, based on optimization of C, Mo and W, partial substitution of Mo by W, and addition of Co, Ta, Nd, has been developed to allow the application above 923 K<sup>6,8</sup>.

Microstructure of 9~12 wt.% Cr ferritic creep steels, as generally composed by tempered martensite matrix and 6~8% delta ferrite, is stabilized by solution strengthening and precipitation strengthening. During long term aging at high temperature, the microstructural evolutions can be described as follows: recovery of martensite matrix (growth of martensitic lath), coarsening of precipitates ( $M_{23}C_6$ ), precipitation of new brittle intermetallic phases (Laves phases, Z-phase) on grain boundaries and subgrain (martensite lath) boundaries<sup>9–12</sup>. The coarsening of precipitates and the precipitation of new brittle intermetallic phases are deemed to result in the microstructural instability, deteriorate the creep strength and the fracture properties.  $M_{23}C_6$  second phase is considered to mainly precipitates on prior austenite grain boundaries and martensitic subgrain boundaries, and act as an obstacle of boundaries migration<sup>13</sup>. However, the coarsening of  $M_{23}C_6$  particles tends to be easy during aging due to the large solubility of Fe and Cr as the major composed elements of  $M_{23}C_6$ .  $M_{23}C_6$  particles are general considered to play a major role on the stabilization of the tempered martensite lath structure, comparing to MX and Laves phase, and thus, prevention of coarsening of  $M_{23}C_6$  particles is important for creep strength improvement<sup>14,15</sup>.

Laves phase, composed by  $[(Fe, Cr)_2(W, Mo)]$ , only appears during aging/creep<sup>16,17</sup>. The precipitation of Laves phase during long term aging leads to a depletion of W and Mo as the solid solution strengthening elements in the matrix, and, thereby, to a reduction of the solid solution strengthening in 9~12 wt.% Cr ferritic creep steels.

<sup>1</sup>School of Materials Science and Engineering, Northeastern University, Shenyang, 110819, China. <sup>2</sup>Research and Development Department, CITIC Bohai Aluminium Industries Holding Company, LTD., Qinhuangdao, 066000, China. <sup>3</sup>School of Economics and Management, Yanshan University, Qinhuangdao, 066004, China. <sup>4</sup>School of Mechanical, Materials and Mechatronic Engineering, University of Wollongong, Wollongong, NSW 2522, Australia. Correspondence and requests for materials should be addressed to Q.G. (email: [neuqgao@163.com](mailto:neuqgao@163.com)) or H.L. (email: [huijun@uow.edu.au](mailto:huijun@uow.edu.au))

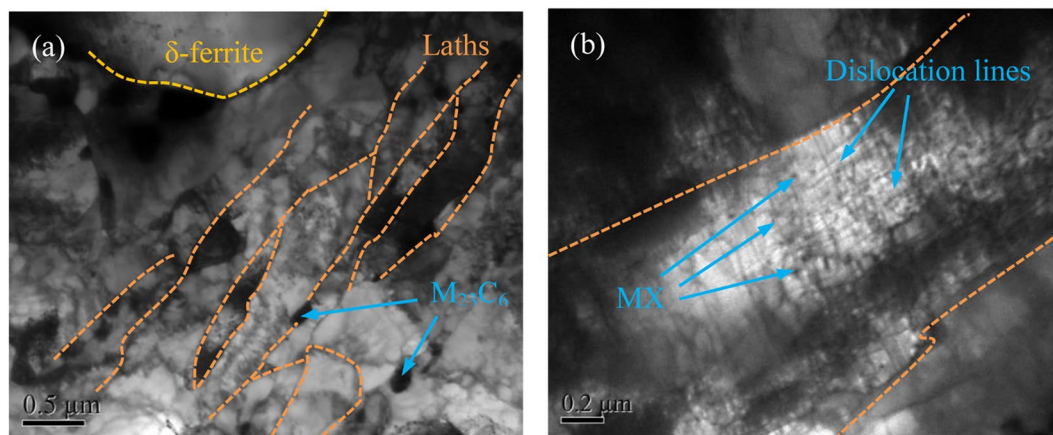


**Figure 1.** TEM micrographs of 9Cr-1.7W-0.4Mo-Co ferritic steel after isothermal aging for 500h, total microstructure (a) and details in martensite lath (b).

Whereas, Laves phase with small particle size also can increase the creep strength by precipitation hardening at early stage of aging/creep<sup>18–20</sup>. In addition, compared to  $M_{23}C_6$  and Laves phase, MX carbonitrides (i.e.,  $M = \text{metals}$ ,  $X = \text{C/N}$ ) exhibit the smallest size, and mainly distribute at subgrain boundaries and within martensite laths<sup>21,22</sup>. Chen *et al.*<sup>23</sup> showed that martensite laths with the finely dispersed nanosized MX in 9wt.% Cr ferritic steel would contribute to the improvement of high-temperature mechanical performance. Panait *et al.*<sup>22</sup> displayed that MX carbonitrides are very stable during thermal and creep exposure of P91 steel at 873 K up to  $10^5$  h.

According to Zener pinning equation, the pinning effort of the particles is related to particle size and distance between each other<sup>24,25</sup>. Based on this, the pinning forces of MX carbonitrides should be higher than that of  $M_{23}C_6$  carbides. Furthermore, Some references<sup>26,27</sup> also proved that MX carbonitrides in 9 wt.% Cr ferritic steel were more advantageous than  $M_{23}C_6$  carbides because MX precipitated finely and densely, and did not coarsen easily at high temperatures. Factually, MX carbonitrides effectively strengthen boundaries because they can act as obstacles to migrating boundaries<sup>28</sup>, and are very stable during short aging/creeping. Thus, in the case of without considering the evolution of MX carbonitrides, the coarsening of  $M_{23}C_6$  particles and the formation of Laves phase, both as the key factors that will affect the microstructural stability of 9–12 wt.% Cr ferritic creep steels during aging/creep, especially 9 wt.% Cr creep strengthening steel with addition of Co, should be given more enough data to find ways for improving the aging/creep strength of the steels.

The content of delta ferrite in 9–12 wt.% Cr ferritic creep steels can be influenced by the alloy elements as W, Mo, Co, *etc.*, especially as C<sup>29</sup>. The diagram of transformed phase (delta ferrite) as a function of net chromium equivalent (NCE) has been characterized in some references<sup>29,30</sup>. For example, there is no delta ferrite in T91 ferritic steel, but it is up to 6–8% in modified ferritic steel with Co addition and elements adjustment<sup>31,32</sup>. With the situation of high content, delta ferrite plays important roles on solid solution strengthening of alloying elements and precipitation behavior of secondary phases, such as  $M_{23}C_6$  and Laves phase. The dissolved alloying elements (such as Cr, C, W, Mo, and so on) contents in delta ferrite matrix are theoretically higher than that in martensite for the tempered samples, which will promote the formation of the precipitates<sup>33–35</sup>. Whereas, the solidifications of other alloying elements, such as Co, Mn and Ni, are crucial in hindering the formation of delta ferrite<sup>33,36</sup>. The works in our previous researches also proved that the content Redjaimia *et al.*<sup>37</sup> showed that the precipitation of  $M_{23}C_6$  phase prior to the other precipitates on delta ferrite boundaries, which is always attributed to the high mobility of carbon towards the boundaries enriched in  $M_{23}C_6$  forming alloying elements. In addition, accompanying with precipitation of secondary phases, the structure of delta ferrite has been changed, and some dislocations should be found in the interior of delta ferrite, which is rarely reported and explained.

The microstructural evolution and the distribution of alloying elements of the new modified 9Cr-1.7W-0.4Mo-Co ferritic heat-resistant steel during isothermal aging were described in our previous article<sup>35</sup>. This article presents a detailed description of the precipitation behavior in the same aged steel. The powder of the precipitates is obtained by electrolytic phase extraction (EPE) technology, and analyzed using scanning electron microscope (SEM), transmission electron microscopy (TEM) and X-ray diffraction (XRD).  $M_{23}C_6$  and Laves phase were identified by the selected area diffraction (SAD). The particle size distribution and the coarsening kinetics of  $M_{23}C_6$  precipitates were also analyzed.

## Results

**Microstructural evolutions on delta ferrite boundaries.** TEM micrographs of 9Cr-1.7W-0.4Mo-Co ferritic steel aged for 500 h are displayed in Fig. 1. Martensite consists of laths and delta ferrite can be distinguished, and some  $M_{23}C_6$  precipitates with large particles distributed at martensite lath boundaries and the interface of delta ferrite and martensite. In addition, nano-sized MX precipitates were homogeneously distributed in martensite lath, which would impede the migration of high-density dislocations and insist stable microstructure during isothermal aging (seen in Fig. 1b).

As we discussed in our previous works<sup>35,38</sup>, there were many precipitates particles located at the interface of delta ferrite and martensite in ferritic heat-resistant steels. The delta ferrite, enriched in BCC stabilising alloying

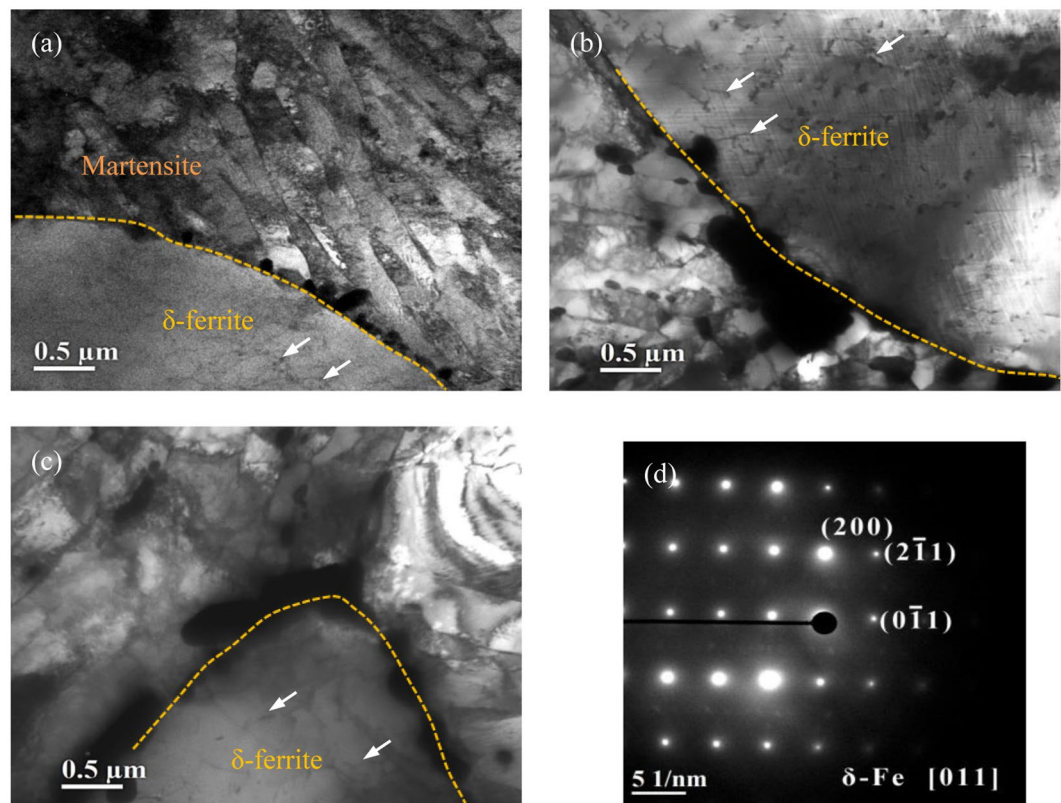


**Figure 2.** TEM images of precipitates located at the interface of delta ferrite and martensite in 9Cr-1.7W-0.4Mo-Co ferritic steel after isothermal aging for 100h (a), 500h (b), 1000h (c), and SAD result of delta ferrite (d).

elements, notably Cr, Mo and W, is a favourable site for some precipitates, such as  $M_{23}C_6$ , Laves phase, comparing to austenite and martensite. Therefore, it means that the alloying elements, which are contributed to the formation of precipitates located at the boundaries of delta ferrite grain, are provided by delta ferrite phase. During aging, the migrations of alloying elements from the interior to the grain boundaries of delta ferrite phase lead to the formation of precipitates with a large number, and new dislocations located in the interior of delta ferrite phase might be emerged.

Figure 2 shows TEM images of delta ferrite containing in 9Cr-1.7W-0.4Mo-Co ferritic steel after isothermal aging for different time. There are three obvious characters can be distinguished as follows:

- (i) Some isolated dislocations (as marked by the light arrows in Fig. 2) were detected in the delta ferrite grains during isothermal aging, and the dislocation density kept to be increased with the increase in aging time. The atoms of dissolved alloying elements migrate from the interior to the boundary of delta ferrite, and form the precipitates located at the grain boundaries with the duration of isothermal aging, which means that many lattice vacancies are remained in delta ferrite grains.
- (ii) The density of the precipitates located on the interface of martensite and delta ferrite was obviously higher, comparing to which located at the boundaries of martensite laths. This also can be attributed to that there is a relatively high density of dissolved alloying elements in delta ferrite, which is beneficial to the formation of precipitates, and also indicating that the particle size of precipitates at the interface should be larger.
- (iii) Most of the particles of precipitates grew into martensite laths with the duration of isothermal aging, only partially small particles would inversely intrude into delta ferrite grains.

**Compositions of the precipitates.** The powder of the precipitates in the aged 9Cr-1.7W-0.4Mo-Co ferritic steel obtained by EPE technology was analyzed using routine X-ray diffraction, as shown in Fig. 3. In the all XRD patterns, the remarkable peaks were clearly visible, and which could be identified as the Cr-rich carbide of an  $M_{23}C_6$  type, *i.e.*,  $Cr_{23}C_6$  phase. Additionally, the peaks around 2-theta angles  $35^\circ$  and  $71^\circ$  represented an MX type precipitate enriched in Nb (NbC phase), which has also been detected from the XRD patterns.  $Fe_2W$  Laves phase was not identified until the time of isothermal aging was extended to about 2000 h. In our previous research, the increase in W element content in some areas, such as grain boundaries and around  $M_{23}C_6$  particles, is beneficial to match the formation of  $Fe_2W$  Laves phase with the duration of isothermal aging<sup>35</sup>. Therefore, the migration and enrichment of W element on the grain boundaries or around the  $M_{23}C_6$  particles during aging result in the formation of  $Fe_2W$  phase.

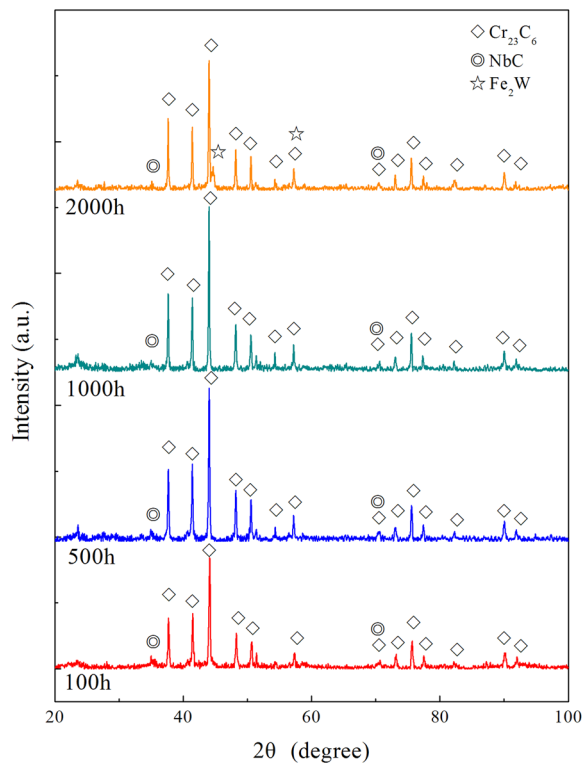


**Figure 3.** X-ray diffraction patterns of the precipitates obtained by electrolytic phase extraction in 9Cr-1.7W-0.4Mo-Co ferritic steel subjected to isothermal aging.

The energy dispersive spectroscopy (EDS) analyses of alloying elements distributions in the microstructure of the material subjected to isothermal aging for 2000 h are displayed in Fig. 4. Some subgrains can be observed with the duration of aging. The large and small precipitates particles were located on the subgrain boundaries and in the interior of subgrains. It can be seen that the alloying elements distributions among different particles are obviously heterogeneous. The high densities of Cr, C and W alloying elements distribute in the large particles with ellipsoidal and spherical shapes located at the subgrain boundaries, which indicates that the large particles can be identified as  $M_{23}C_6$  precipitates enriched in Cr element. Several ellipsoidal particles enriched in W element and depleted in Cr element should be considered as  $Fe_2W$  Laves phase (as shown by yellow arrows in Fig. 4). The content of Fe element in the  $Fe_2W$  Laves phase was lower comparing to the Fe-matrix phase (martensite), which also should be noted.

Figure 5a and b represent TEM micrograph and EDS results of the precipitates powder extracted from 9Cr-1.7W-0.4Mo-Co ferritic steel after 100 h aged. The ellipsoidally shaped particles with 200 nm and 65 nm in long axis and short axis, respectively, and a plate-shaped particle with 400 nm in length, can be obviously distinguished. The chemical compositions of these particles are similar to each other, containing high Cr and Fe contents with traces of W and Mo as shown in Fig. 5b. The selected area diffraction (SAD) patterns of the particles marked in Fig. 5a are displayed in Fig. 5c and d, identifying that both the particles with the two shapes are face-centered cubic structure (FCC),  $Cr_{23}C_6$  precipitates. For the case of 9Cr-1Mo ferritic steel, it has already been established that the composition, size, and distribution of  $M_{23}C_6$  precipitates are mainly dependent on ageing time and temperature: a longer time and higher ageing temperature are considered to induce equilibrium and hence a higher volume fraction of the precipitates<sup>39</sup>. Whereas, a long duration such as after 1000 h may mark the onset of carbide particle coarsening and the appearance of new brittle phases such as Laves and Z-phase<sup>11, 20</sup>.

Figure 6 shows TEM analysis of Laves phase formed in the 9Cr-1.7W-0.4Mo-Co ferritic steel after isothermal aging for 2000 h. It should be pointed out that there is no Laves phase being found in other samples, such as aging for 1000 h, which means that the microstructure of the ferritic steel is still very stable during long-termed aging. The particle size of laves phase is measured to be ~ 200 nm, which is consistent with the literatures<sup>40, 41</sup>.  $Fe_2W$  Laves phase can be identified using SAD and EDS methods. The EDS result indicates that Fe and W are dominant in the Laves phase with traces of Mo and Cr. One mechanism is that the nucleation of Laves phase precipitates at the Cr-depleted regions with relatively high W and Mo contents adjacent to  $M_{23}C_6$  particles. The  $M_{23}C_6$  particles are identified as a composition of  $(Fe, Cr, Mo, W)_{23}C_6$  as we discussed above. Therefore, the alloying elements distributions in  $M_{23}C_6$  particles with the durations of isothermal aging are analyzed by EDS, which can reflect the rearrangement of alloying elements and indicate the formed location of Laves phase, and the results are displayed in Table 1. The content of Cr increases from 53.87 wt.% to 63.31 wt.% in  $M_{23}C_6$  precipitates with the increase in aging time from 100 h to 2000 h, W content inversely decreases from 19.25 wt.% to 11.86 wt.%, both of them show a rearrangement of alloying elements during isothermal aging. It means that the dissolved W in  $M_{23}C_6$  phase will precipitate, and the precipitated W elements in the vicinity of  $M_{23}C_6$  phase are beneficial to the formation of

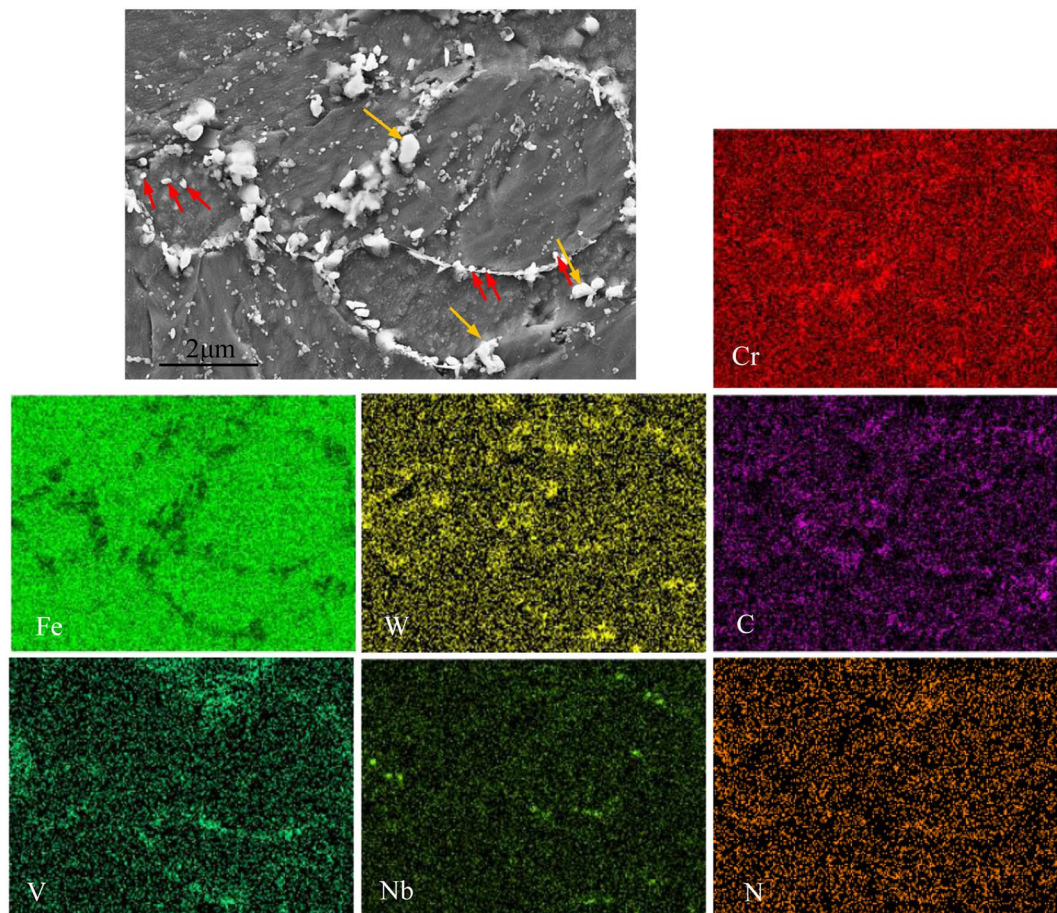


**Figure 4.** SEM and EDS analyses of alloying elements distributions in the microstructure of 9Cr-1.7W-0.4Mo-Co ferritic steel subjected to isothermal aging for 2000h.

$\text{Fe}_2\text{W}$  Laves phase, and thus Laves phase is preferential to precipitate at the locations adjacent to  $\text{M}_{23}\text{C}_6$  particles. In other words, for  $\text{M}_{23}\text{C}_6$  phase during aging, the chemical compositions will be changed due to the formation of Laves phase, except the coarsening of the particle size during aging as reported in the literatures<sup>42,43</sup>.

**Particle size of  $\text{M}_{23}\text{C}_6$ .** Quantification of the particle size distributions of  $\text{M}_{23}\text{C}_6$  phase was carried out based on TEM images of the EPE samples, and thus it is difficult to distinguish the location of  $\text{M}_{23}\text{C}_6$  phase. To obtain sufficiently accurate statistics for the particle size distributions, the number of particles counted using computer-aided software was above 300. Employing Banerjee's method<sup>44</sup>, it is assumed that  $A$  represents the particle area, and the equivalent area diameter (EQAD),  $d_A$ , can be given as:

$$d_A = \sqrt{\frac{4A}{\pi}} \quad (1)$$

The particle diameter was obtained by using the measured particle area in Eq. (1). Hence, the obtained particle size distributions as a function of particle diameter are displayed in Fig. 7.

The changes in particle sizes of  $\text{M}_{23}\text{C}_6$  precipitates can be considered to obey the Gaussian distribution in total. However, the distributions of particle sizes with ranges of 50~180 nm and 50~220 nm for the samples subjected to aging for 100 h and 500 h, respectively, are more uniform, comparing to the samples with a longer duration of ageing time (1000 h and 2000 h). With the increase in aging time to 1000 h, most of particle sizes increased to a range of 100~240 nm, indicating that  $\text{M}_{23}\text{C}_6$  precipitates with small size are preferential to coarsen firstly, and the large  $\text{M}_{23}\text{C}_6$  are relatively stable during short aging. The reason can be attributed to the distributions of alloying elements adjacent to  $\text{M}_{23}\text{C}_6$  particles. The alloying elements, such as Cr and C around small  $\text{M}_{23}\text{C}_6$  particles, can be considered to be homogeneous, which means that there are enough elements to migrate into  $\text{M}_{23}\text{C}_6$  particles and promote the coarsening of precipitates. For large  $\text{M}_{23}\text{C}_6$  particles, whereas, the existence of Cr depleted area will partly decrease the coarsening progress of  $\text{M}_{23}\text{C}_6$  phase.

## Discussion

Theoretically, the alloying elements, formed the precipitates located on the interface of martensite and delta ferrite, are from the interior of delta ferrite, and thus the precipitate particles should be inclined to grow into delta

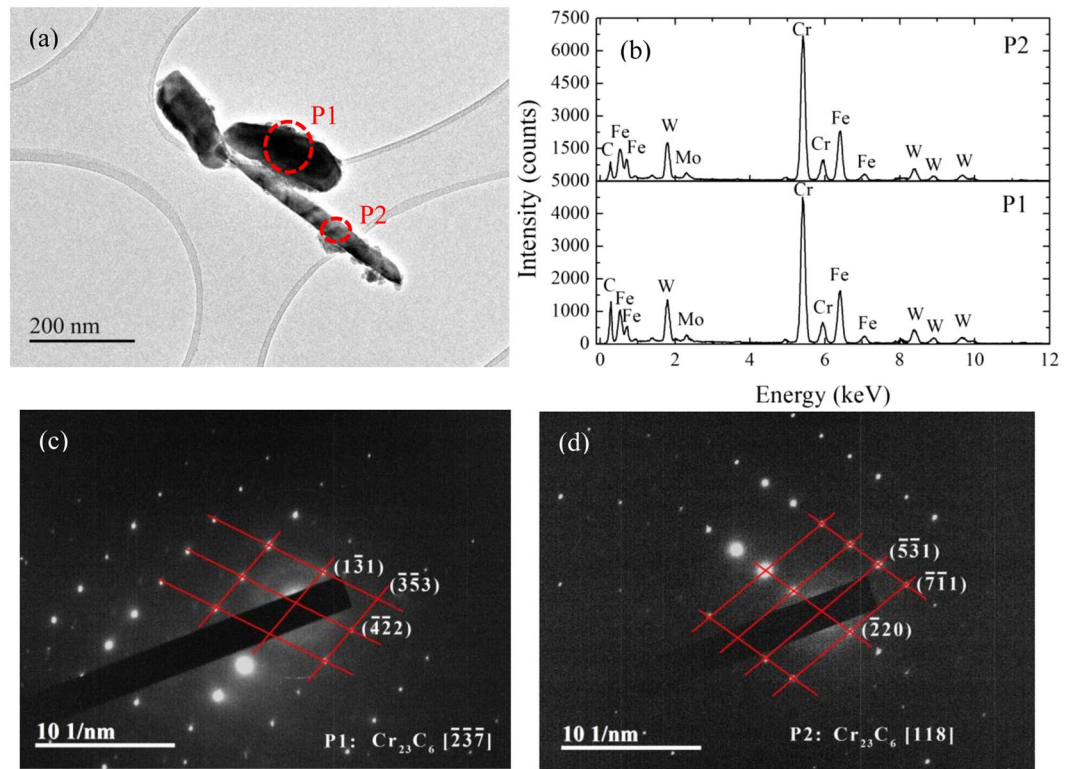


**Figure 5.** TEM image (a), EDS results (b) and the selected area diffractions marked with “P1” (c) and “P2” (d) of the precipitates in 9Cr-1.7W-0.4Mo-Co ferritic steel after isothermal aging for 100 h, showing  $M_{23}C_6$  precipitates.

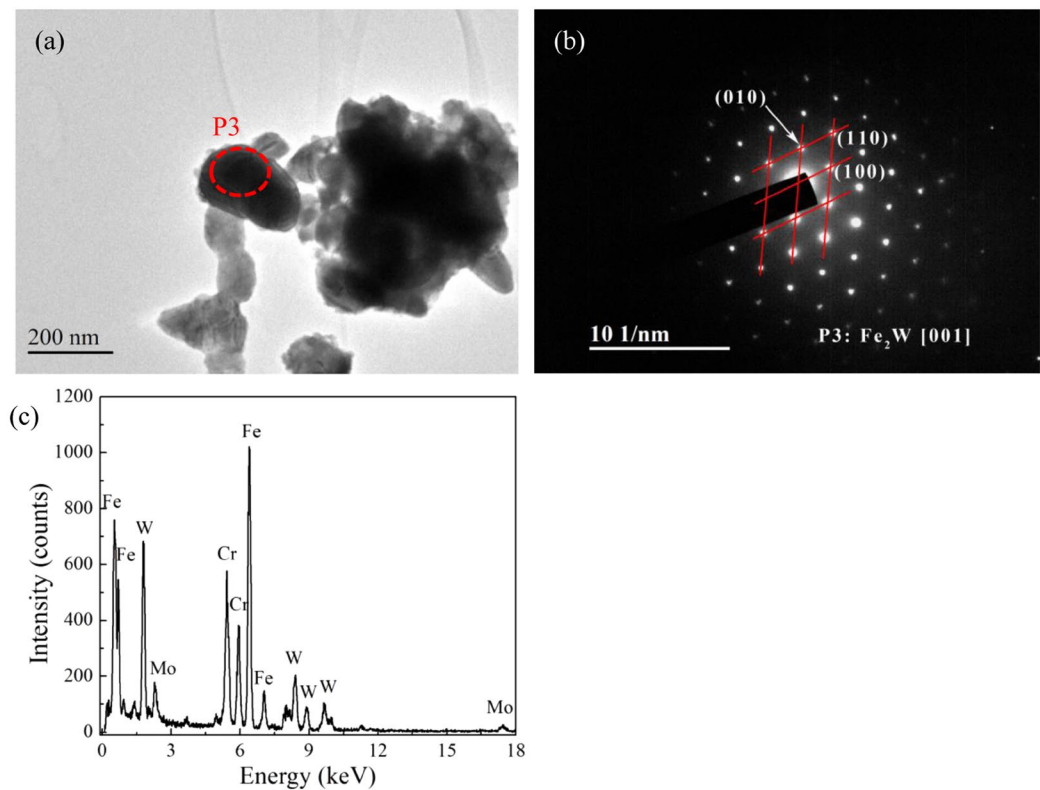


**Figure 6.** TEM image (a), SAD (b) and EDS result (c) of Laves phase (marked with “P3”) in 9Cr-1.7W-0.4Mo-Co ferritic steel after isothermal aging for 2000 h.

	Fe	Cr	W	Mo	Nb	V
100h	21.48	53.87	19.25	4.32	0.22	0.86
500h	20.34	59.28	15.18	3.86	0.25	1.08
1000h	22.98	60.01	13.52	2.70		0.79
2000h	19.11	63.31	11.86	4.44	0.10	1.18

**Table 1.** Alloying elements contents in  $M_{23}C_6$  precipitates of 9Cr-1.7W-0.4Mo-Co ferritic steel after isothermal aging (mass%).

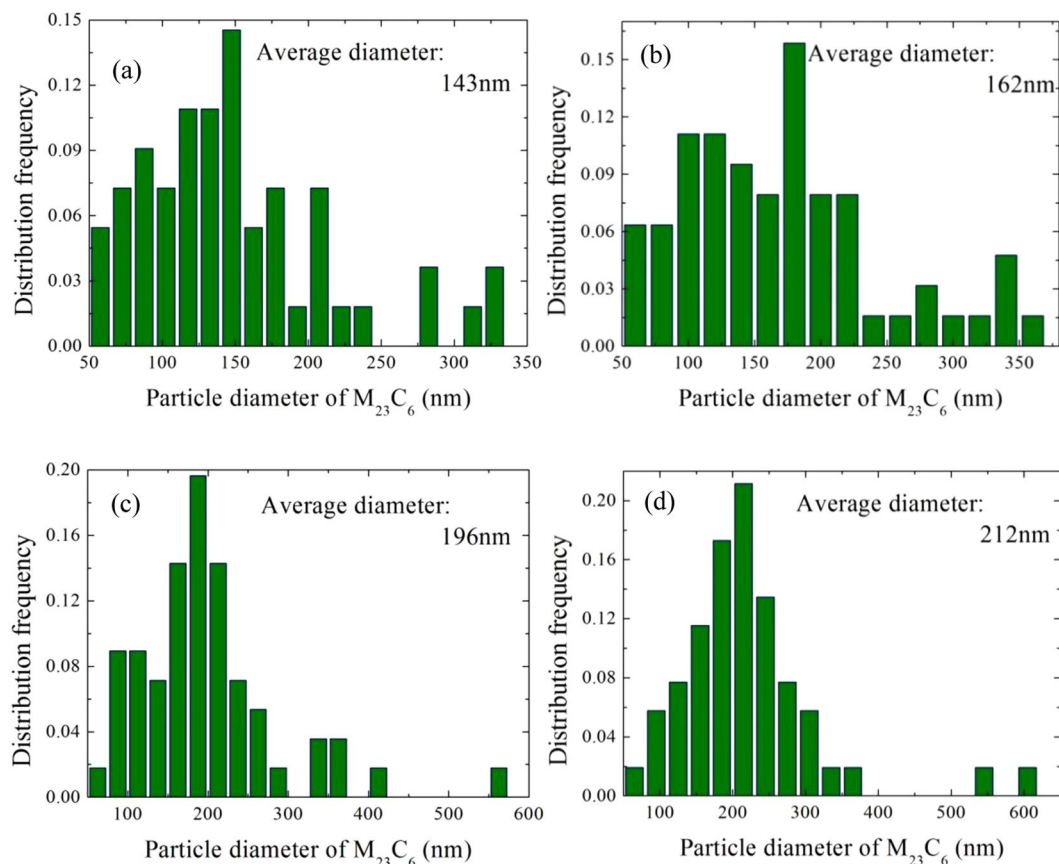


**Figure 7.** Distribution frequency as a function of particle diameter of  $M_{23}C_6$  precipitates in 9Cr-1.7W-0.4Mo-Co ferritic steel after isothermal aging for 100h (a), (b) 500h (b), 1000h (c), 2000h (d), counting from TEM images of the EPE samples.

ferrite. In fact, the original interface of martensite and delta ferrite has migrated into the delta ferrite with the diffusion of atoms, and advances ahead of the precipitates particles, which will leave the precipitates as isolated particles in the martensite. The migration of delta ferrite interface depends not only on the chemical composition, but also to some extent on the temperature which affect the diffusion rate of atoms as reported in the literatures<sup>45–47</sup>. When the aging temperature is to be above 873 K, it is considered that the migration of  $\delta/\alpha'$  interface is obviously ahead of the growth of the precipitates<sup>45</sup>. Hence, the precipitates were retained in martensite due to the migration of  $\delta/\alpha'$  interface during aging at 973 K which can be seen in Fig. 2.

In our previous works, the alloying elements comparisons between different phases have been accomplished, and the results showed that the contents of Fe in martensite, delta ferrite and precipitates were about 85.9 wt.%, 89.6 wt.% and 36.5 wt.%, respectively<sup>35</sup>. The highest content of Fe in matrix phase is easy to be understood. Besides, the MX-type precipitates enriched in Nb located on the subgrain boundaries and in the interior of subgrains also can be recognized, respectively (as shown by red arrows in Fig. 4). During aging/creep, Laves phase precipitated on grain or subgrain (martensite lath) boundaries has been proved that it will reduce the efficiency of grain boundary as a sink of dislocations, and suppresses the recovery of dislocations at grain boundaries<sup>41, 48</sup>. Nevertheless, the small particle size of Laves phase improves the pinning force of the migrations of dislocations and grain boundaries, and increases the stability of microstructure, which means that the role of Laves phase with this situation is similar to  $M_{23}C_6$  and MX<sup>49, 50</sup>. As seen in Fig. 4, the average particle size of Laves phase is about

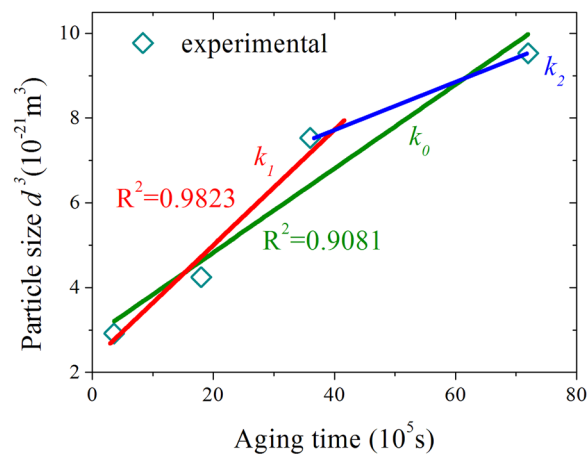


**Figure 8.** Coarsening of  $M_{23}C_6$  particles in 9Cr-1.7W-0.4Mo-Co ferritic steel aging at 973 K, the cubic of measured average particle diameter and fitted curve as a function of aging time.

200~500 nm, which is same to  $M_{23}C_6$  particles, indicating that the microstructure of the materials aged for 2000 h should be still stable due to precipitation strengthening of the precipitates.

$M_{23}C_6$  particle coarsening as a function of aging time has been studied in ferritic heat-resistant steels and other alloys<sup>42, 51-53</sup>. The particle coarsening rate for  $M_{23}C_6$  phase so far follows the equations based on the classical Lifshitz-Slyozov-Wagner (LSW) theory which assumes supersaturated solid solution, misfit-free spherical particles, and one-rate controlling solute<sup>51, 54, 55</sup>. According to LSW theory, the coarsening kinetics of the particles for volume diffusion-controlled growth processes follows the law:

$$d^3 - d_0^3 = kt \quad (2)$$

where  $d$  and  $d_0$  correspond to the average particle diameter at aging time  $t$  and the initial average particle diameter, respectively, and  $k$  is the coarsening rate constant with a formula as<sup>56</sup>:

$$k = \frac{8C_e V_m D \Omega}{9RT} \quad (3)$$

with  $C_e$  as the equilibrium concentration of atom in the matrix,  $V_m$  as the molar volume of the precipitates,  $D$  as the diffusion coefficient of atom in the matrix,  $\Omega$  as the interfacial energy of precipitates/matrix,  $R$  as the gas constant, and  $T$  as the aging temperature in K.

The average particle diameters of  $M_{23}C_6$  phase aged at 100 h, 500 h, 1000 h and 2000 h are 143 nm, 162 nm, 196 nm and 212 nm as obtained from Fig. 7, respectively. Hence, the cubic of average particle diameter as a function of aging time in second (s) is shown in Fig. 8. The Laves phase is consisted with the same alloying elements, such as Fe, W, Mo and Cr, as  $M_{23}C_6$  phase except for C. According to Gustafson<sup>57</sup>, the  $M_{23}C_6$  coarsening should be higher if the Laves phase is not allowed to form, comparing to the situation that when the amount of Laves phase has an equilibrium amount. The other researchers inversely showed that the formation of Laves phase does not affect much the coarsening of  $M_{23}C_6$ <sup>58</sup>. There is no Laves phase can be found until increasing aging time to 2000 h in our work, it means that the influence of Laves phase on the  $M_{23}C_6$  coarsening can be ignored under shorter aging time. A linear relationship between the cubic of average particle diameter and the aging time was determined for aging at 973 K, which approximately satisfies the predictions of LSW theory. The thus coarsening rate constant of  $M_{23}C_6$  phase during aging was determined as  $k_0 = 9.75 \times 10^{-28} \text{ m}^3 \text{ s}^{-1}$  from the slope (green fitted line). Whereas, the R-square value is about 0.9081, indicating that the fitting result is not accurate. In fact, Laves phase is found in the sample aging for 2000 h, the initial nucleation/formation stage of Laves phase is still unknown. In addressing, two stages of  $M_{23}C_6$  coarsening without and with the effect of Laves Phase are considered. Therefore, the first stage is under the assumption that the Laves phase was not allowed to form at all, *i.e.*, from the aging beginning to about 1000 h, and the coarsening rate of  $M_{23}C_6$  is about  $k_1 = 1.21 \times 10^{-27} \text{ m}^3 \text{ s}^{-1}$  with a higher R-square of 0.9823. The second stage in our work should be considered to be from 1000 h to 2000 h with the coarsening rate of  $k_2 = 4.52 \times 10^{-28} \text{ m}^3 \text{ s}^{-1}$ . The results indicate that the formation of Laves phase will affect the coarsening of  $M_{23}C_6$  phase.

The coarsening rates of  $M_{23}C_6$  particle at the range from 873 K to 1023 K deduced from data in references and this work are listed in Table 2. As we know, the coarsening rate of  $M_{23}C_6$  particle is mainly dependent on aging/creep temperature, and theoretically increases with the increase in temperature for the same materials, which is obviously identified in Table 2. The lowest coarsening rate is only  $0.088 \times 10^{-29} \text{ m}^3 \text{ s}^{-1}$  in modified 9%Cr Steel with 1% Co at 873 K. Considering the existence of Laves phase at exposing temperature 973 K, the  $M_{23}C_6$  coarsening is relatively low in 9Cr-1.7W-0.4Mo-Co ferritic steel, comparing to 12%Cr steel and H13 steel, indicating that  $M_{23}C_6$  phase in our materials is stable at 973 K.



Temperature (K)	Coarsening rate ( $\times 10^{-29} \text{m}^3 \text{s}^{-1}$ )	Materials
873	0.088	9%Cr Steel with 1% Co <sup>36</sup>
	0.12	P92 steel <sup>5</sup>
	1.03	P92 steel <sup>57</sup>
923	0.546	12%Cr steel <sup>51</sup>
	1.37	P92 steel <sup>5</sup>
	1.8	9% Cr Steel with 1% Co <sup>36</sup>
	25.3	P91 steel <sup>5</sup>
973	76.9	12%Cr steel contains Laves <sup>13</sup>
	$k_0 = 97.5$	this work
	$k_1 = 121$	
	$k_2 = 45.2$	
	530	H13Nb steel <sup>42</sup>
	760	H13 steel <sup>42</sup>
1023	21.1	12%Cr steel <sup>51</sup>
	450	9% Cr Steel with 1% Co <sup>36</sup>

**Table 2.** Coarsening rates of  $M_{23}C_6$  particle at the range from 873 K to 1023K obtained in references and this work.

Element	C	Si	Mn	Cr	Mo	W	V	Nb	N	Co	B	Ti	Al
wt.%	0.05	0.21	0.44	9.81	0.43	1.73	0.22	0.07	0.03	1.21	0.0045	<0.01	0.014

**Table 3.** Chemical compositions of the modified high Cr ferritic heat-resistant steel (mass%).

## Methods

Material used in the present work is a new modified ferritic heat-resistant steel, 9Cr-1.7W-0.4Mo-Co steel subject to being hot-rolled to 12 mm thick at 1373 K, and then tempered at 1023 K for 2 h. The chemical composition of the steel was determined by Inductive Coupled Plasma-Optical Emission Spectrometry (ICP-OES), and the thus obtained results are listed in Table 3. Further, the tempered steel was cut to several small pieces which were isothermally aged at 973 K holding for 100 h, 500 h, 1000 h and 2000 h, respectively. The aging tests were conducted in a vacuum tube furnace with a temperature tolerance of  $\pm 5^\circ\text{C}$ , and a vacuum degree of  $-0.09 \text{MPa}$  in the furnace was controlled to avoid oxidation.

Characterization of microstructure was realized by SEM (ZEISS, SUPRA-55) and TEM (JEOL, JEM-2010) at an accelerating voltage of 15 kV and 200 kV, respectively. The specimens for SEM were prepared by mechanical polishing, and then etching in a solution composed by iron trichloride (5 g), hydrochloric acid (20 mL) and distilled water (100 mL). Thin foils with 130–150 micrometers for TEM were prepared by a twin-jet electropolisher using a solution of 10% perchloric acid and 90% ethanol.

Electrolytic phase extraction (EPE) technology was employed to analyze the composition of the precipitates. Using EPE, the matrix phase was etched and dissolved in the solution, and only the precipitate particles were extracted. EPE of the samples at a current density of  $120 \text{mA/cm}^2$  operated in a solution of 25% hydrochloric acid and 75% alcohol, and then the precipitates powder extracted from the samples were collected on the bottom of the flask after washing 3–5 times with alcohol. The compositions of the powder were identified by XRD analysis using  $\text{Cu K}\alpha$  radiation at room temperature, with a step size of  $0.02^\circ$  and observed by TEM.

## Conclusions

The precipitates in the 9Cr-1.7W-0.4Mo-Co ferritic heat-resistant steel subjected to isothermal aging at 973 K were investigated using SEM, TEM and XRD. The  $M_{23}C_6$  particle coarsening as a function of aging time is also described. The conclusions are summarized as follows:

- (1) The isolated dislocations were detected in delta ferrite interior, and increase with the increase in aging time. Both the density and the particle size of the precipitates on  $\delta/\alpha'$  boundaries are obviously larger than other locations, and the migration of  $\delta/\alpha'$  boundaries leads to the retained precipitates in martensite.
- (2)  $\text{Cr}_{23}\text{C}_6$ , NbC and  $\text{Fe}_2\text{W}$  precipitates are recognized based on XRD, and  $\text{Fe}_2\text{W}$ -Laves phase can only be found as duration of aging time to 2000 h. The precipitated W elements in the vicinity of  $M_{23}C_6$  phase are beneficial to the formation of  $\text{Fe}_2\text{W}$  Laves phase, which shows that Laves phase is preferential to form at the locations adjacent to  $M_{23}C_6$  particles.
- (3)  $M_{23}C_6$  precipitates with small particle size are preferential to coarsen firstly, and the large  $M_{23}C_6$  are relatively stable during short aging.

- (4) The total coarsening rate of  $M_{23}C_6$  precipitates is  $9.75 \times 10^{-28} \text{ m}^3 \text{ s}^{-1}$ , but it changes to  $1.21 \times 10^{-27} \text{ m}^3 \text{ s}^{-1}$  without the formation of Laves phase, and  $4.52 \times 10^{-28} \text{ m}^3 \text{ s}^{-1}$  with consideration of Laves phase, respectively, indicating that the coarsening of  $M_{23}C_6$  precipitates depends on the formation of Laves phase.

## References

- Liu, C., Shao, Y., Chen, J. & Liu, Y. Non-instantaneous growth characteristics of martensitic transformation in high Cr ferritic creep-resistant steel. *Appl. Phys. A* **122**, 1–7 (2016).
- Gao, Q. *et al.* Influence of austenitization temperature on phase transformation features of modified high Cr ferritic heat-resistant steel. *Nucl. Eng. Des.* **256**, 148–152 (2013).
- Nagode, A., Kosec, L., Ule, B. & Kosec, G. Review of creep resistant alloys for power plant applications. *Metallurgija* **50**, 45–48 (2011).
- Gao, Q., Wang, Y., Gong, M., Qu, F. & Lin, X. Non-isothermal austenitic transformation kinetics in Fe–10Cr–1Co alloy. *Appl. Phys. A* **122**, 1–10 (2016).
- Hald, J. & Korcakova, L. Precipitate Stability in Creep Resistant Ferritic Steels-Experimental Investigations and Modelling. *ISIJ Int.* **43**, 420–427 (2003).
- Knežević, V., Balun, J., Sauthoff, G., Inden, G. & Schneider, A. Design of martensitic/ferritic heat-resistant steels for application at 650 °C with supporting thermodynamic modelling. *Mater. Sci. Eng., A* **477**, 334–343 (2008).
- Yamamoto, K., Kimura, Y. & Mishima, Y. Effect of matrix microstructure on precipitation of Laves phase in Fe–10Cr–1.4 W (–Co) alloys. *Intermetallics* **14**, 515–520 (2006).
- Vanaja, J. *et al.* Creep deformation and rupture behaviour of 9Cr–1W–0.2V–0.06Ta Reduced Activation Ferritic–Martensitic steel. *Mater. Sci. Eng., A* **533**, 17–25 (2012).
- Hattestrand, M. & Andrén, H. O. Microstructural development during ageing of an 11% chromium steel alloyed with copper. *Mater. Sci. Eng., A* **318**, 94–101 (2001).
- Ghassemi-Armaki, H., Chen, R., Maruyama, K., Yoshizawa, M. & Igarashi, M. Static recovery of tempered lath martensite microstructures during long-term aging in 9–12% Cr heat resistant steels. *Mater. Lett.* **63**, 2423–2425 (2009).
- Danielsen, H. K. & Hald, J. A thermodynamic model of the Z-phase Cr (V, Nb) N. *Calphad* **31**, 505–514 (2007).
- Prat, O., Garcia, J., Rojas, D., Carrasco, C. & Inden, G. Investigations on the growth kinetics of Laves phase precipitates in 12% Cr creep-resistant steels: Experimental and DICTRA calculations. *Acta Mater.* **58**, 6142–6153 (2010).
- Xiao, X., Liu, G., Hu, B., Wang, J. & Ma, W. Coarsening behavior for M<sub>23</sub>C<sub>6</sub> carbide in 12%Cr-reduced activation ferrite/martensite steel: experimental study combined with DICTRA simulation. *J. Mater. Sci.* **48**, 5410–5419 (2013).
- Ghosh, S. The role of tungsten in the coarsening behaviour of M<sub>23</sub>C<sub>6</sub> carbide in 9Cr–W steels at 600 °C. *J. Mater. Sci.* **45**, 1823–1829 (2010).
- Prat, O., Garcia, J., Rojas, D., Carrasco, C. & Kaysser-Pyzalla, A. R. Investigations on coarsening of MX and M<sub>23</sub>C<sub>6</sub> precipitates in 12% Cr creep resistant steels assisted by computational thermodynamics. *Mater. Sci. Eng., A* **527**, 5976–5983 (2010).
- Wang, X. *et al.* Laves-phase evolution during aging in fine grained heat-affected zone of a tungsten-strengthened 9% Cr steel weldment. *J. Mater. Process. Technol.* **219**, 60–69 (2015).
- Zhou, X., Liu, Y., Liu, C. & Ning, B. Evolution of creep damage in a modified ferritic heat resistant steel with excellent short-term creep performance and its oxide layer characteristic. *Mater. Sci. Eng., A* **608**, 46–52 (2014).
- Shim, J. *et al.* Numerical simulation of long-term precipitate evolution in austenitic heat-resistant steels. *Calphad* **34**, 105–112 (2010).
- Yamamoto, K., Kimura, Y. & Mishima, Y. Effect of matrix microstructure on precipitation of Laves phase in Fe–10Cr–1.4W(–Co) alloys. *Intermetallics* **14**, 515–520 (2006).
- Dimmler, G., Weinert, P., Kozeschnik, E. & Cerjak, H. Quantification of the Laves phase in advanced 9–12% Cr steels using a standard SEM. *Mater. Charact.* **51**, 341–352 (2003).
- Zhou, Y.-H., Liu, C.-X., Liu, Y.-C., Guo, Q.-Y. & Li, H.-J. Coarsening behavior of MX carbonitrides in type 347H heat-resistant austenitic steel during thermal aging. *Int. J. Min. Met. Mater.* **23**, 283–293 (2016).
- Panaït, C. G. *et al.* Evolution of dislocation density, size of subgrains and MX-type precipitates in a P91 steel during creep and during thermal ageing at 600 °C for more than 100,000 h. *Mater. Sci. Eng., A* **527**, 4062–4069 (2010).
- Chen, L., Zeng, Z., Zhao, Y., Zhu, F. & Liu, X. Microstructures and High-Temperature Mechanical Properties of a Martensitic Heat-Resistant Stainless Steel 403Nb Processed by Thermo-Mechanical Treatment. *Metall. Mater. Trans. A* **45**, 1498–1507 (2014).
- Zener, C. Theory of growth of spherical precipitates from solid solution. *J. Appl. Phys.* **20**, 950–953 (1949).
- Manohar, P. A., Ferry, M. & Chandra, T. Five Decades of the Zener Equation. *ISIJ Int.* **38**, 913–924 (1998).
- Taneike, M., Sawada, K. & Abe, F. Effect of carbon concentration on precipitation behavior of M<sub>23</sub>C<sub>6</sub> carbides and MX carbonitrides in martensitic 9Cr steel during heat treatment. *Metall. Mater. Trans. A* **35**, 1255–1262 (2004).
- Zhou, X., Liu, Y., Liu, C., Yu, L. & Li, H. Formation and evolution of precipitates in high Cr ferritic heat-resistant steels. *Mater. Res. Innovations* **19**, S193–S198 (2015).
- Zhou, X., Liu, C., Yu, L., Liu, Y. & Li, H. Phase transformation behavior and microstructural control of high-Cr martensitic/ferritic heat-resistant steels for power and nuclear plants: a review. *Journal of Materials Science & Technology* **31**, 235–242 (2015).
- George, G., Shaikh, H., Parvathavarthini, N., George, R. P. & Khatak, H. S. On the microstructure polarization behavior correlation of a 9Cr–1Mo steel weld joint. *J. Mater. Eng. Perform.* **10**, 460–467 (2001).
- Gao, Q., Liu, Y., Di, X., Dong, Z. & Yan, Z. The isochronal  $\delta \rightarrow \gamma$  transformation of high Cr ferritic heat-resistant steel during cooling. *J. Mater. Sci.* **46**, 6910–6915 (2011).
- Gao, Q., Liu, Y., Di, X., Yu, L. & Yan, Z. Martensite transformation in the modified high Cr ferritic heat-resistant steel during continuous cooling. *J. Mater. Res.* **27**, 2779–2789 (2012).
- Liu, C., Liu, Y., Zhang, D., Gao, Z. & Yan, Z. Bainite formation kinetics during isothermal holding in modified high Cr ferritic steel. *Metall. Mater. Trans. A* **44**, 5447–5455 (2013).
- Klotz, U. E., Solenthaler, C. & Uggowitzer, P. J. Martensitic-austenitic 9–12% Cr steels—Alloy design, microstructural stability and mechanical properties. *Mater. Sci. Eng., A* **476**, 186–194 (2008).
- Bhadeshia, H. K. D. H. Design of Ferritic Creep-resistant Steels. *ISIJ Int.* **41**, 626–640 (2001).
- Gao, Q. *et al.* Microstructure and oxidation properties of 9Cr–1.7W–0.4Mo–Co ferritic steel after isothermal aging. *J. Alloys Comp.* **651**, 537–543 (2015).
- Gustafson, Å. & Ågren, J. Possible Effect of Co on Coarsening of M<sub>23</sub>C<sub>6</sub> Carbide and Orowan Stress in a 9% Cr Steel. *ISIJ Int.* **41**, 356–360 (2001).
- Redjaimia, A., Metauer, G. & Gantois, M. Decomposition of Delta Ferrite in an Fe–22 Cr–5 Ni–3 Mo–0.03 C Duplex Stainless Steel. A Morphological and Structural Study. *Duplex Stainless Steels'91* **1**, 119–126 (1991).
- Gao, Q., Di, X., Liu, Y. & Yan, Z. Recovery and recrystallization in modified 9Cr–1Mo steel weldments after post-weld heat treatment. *Int. J. Pres. Ves. Pip.* **93**, 69–74 (2012).
- Jeyaganesh, B., Raju, S., Murugesan, S., Mohandas, E. & Vijayalakshmi, M. A study on the effect of thermal ageing on the specific-heat characteristics of 9Cr–1Mo–0.1C (mass%) steel. *Int. J. Thermophys.* **30**, 619–634 (2009).

40. Li, Q. Precipitation of Fe<sub>2</sub>W laves phase and modeling of its direct influence on the strength of a 12Cr-2W steel. *Metall. Mater. Trans. A* **37**, 89–97 (2006).
41. Korcakova, L., Hald, J. & Somers, M. A. J. Quantification of Laves phase particle size in 9CrW steel. *Mater. Charact.* **47**, 111–117 (2001).
42. Hu, X., Li, L., Wu, X. & Zhang, M. Coarsening behavior of M<sub>23</sub>C<sub>6</sub> carbides after ageing or thermal fatigue in AISI H13 steel with niobium. *Int. J. Fatigue* **28**, 175–182 (2006).
43. Bjärbo, A. & Hättstrand, M. Complex carbide growth, dissolution, and coarsening in a modified 12 pct chromium steel—an experimental and theoretical study. *Metall. Mater. Trans. A* **32**, 19–27 (2001).
44. Banerjee, K., Militzer, M., Perez, M. & Wang, X. Nonisothermal austenite grain growth kinetics in a microalloyed X80 linepipe steel. *Metall. Mater. Trans. A* **41**, 3161–3172 (2010).
45. Gill, T., Vijayalakshmi, M., Gnanamoorthy, J. & Padmanabhan, K. Transformation of Delta-Ferrite During the Postweld Heat Treatment of Type 316 L Stainless Steel Weld Metal. *Weld. J.* **65**, 122 (1986).
46. Keown, S. R. & Thomas, R. G. Role of delta ferrite in thermal aging of type 316 weld metals. *Met. Sci.* **15**, 386–392 (1981).
47. Dyson, D. J. & Keown, S. R. A study of precipitation in a 12%Cr-Co-Mo steel. *Acta Metallurgica* **17**, 1095–1107 (1969).
48. Cui, H. *et al.* Precipitation behavior of Laves phase in 10% Cr steel X12CrMoWVNbN10-1-1 during short-term creep exposure. *Mater. Sci. Eng., A* **527**, 7505–7509 (2010).
49. Schneider, A. & Inden, G. Simulation of the kinetics of precipitation reactions in ferritic steels. *Acta Mater.* **53**, 519–531 (2005).
50. Abe, F. Precipitate design for creep strengthening of 9% Cr tempered martensitic steel for ultra-supercritical power plants. *Sci. Technol. Adv. Mat.* **9**, 2313–2327 (2008).
51. Vodopivec, F., Steiner-Petrovič, D., Žužek, B. & Jenko, M. Coarsening rate of M<sub>23</sub>C<sub>6</sub> and MC particles in a high chromium creep resistant steel. *Steel Res. Int.* **84**, 1110–1114 (2013).
52. Xu, L.-Q. *et al.* Precipitation behavior and martensite lath coarsening during tempering of T/P92 ferritic heat-resistant steel. *Int. J. Min. Met. Mater.* **21**, 438–447 (2014).
53. Zhao, J.-C., Ravikumar, V. & Beltran, A. Phase precipitation and phase stability in Nimonic 263. *Metall. Mater. Trans. A* **32**, 1271–1282 (2001).
54. Lifshitz, I. M. & Slyozov, V. V. The kinetics of precipitation from supersaturated solid solutions. *J. Phys. Chem. Solids* **19**, 35–50 (1961).
55. Groza, J. R. & Shackelford, J. F. *Materials processing handbook*, 346–352 (CRC press, 2007).
56. Trotter, G. *et al.* Precipitation kinetics during aging of an alumina-forming austenitic stainless steel. *Mater. Sci. Eng., A* **667**, 147–155 (2016).
57. Gustafson, Å. & Hättstrand, M. Coarsening of precipitates in an advanced creep resistant 9% chromium steel—quantitative microscopy and simulations. *Mater. Sci. Eng., A* **333**, 279–286 (2002).
58. Hättstrand, M. & Andren, H. O. Evaluation of particle size distributions of precipitates in a 9% chromium steel using energy filtered transmission electron microscopy. *Micron* **32**, 789–797 (2001).

## Acknowledgements

The grants and financial supports from the National Natural Science Foundation of China (Grant No. 51501034) are gratefully acknowledged. The authors are grateful to Liang Chen and Matthew Franklin (University of Wollongong, NSW, Australia) for kindly experimental technology assistances and discussions.

## Author Contributions

Q.Z.G., Y.N.Z., H.L.Z., H.J.L., C.L., and J.H. participated in the research design, acquisition of data, analysis and interpretation of data, drafting and revising the manuscript. F.Q. undertook the SEM testing and analysis. B.T.W. performed XRD testing. Y.L., and Y.M. participated in TEM testing and data collection. Q.Z.G., H.L.Z., and J.H. wrote the main manuscript text. All authors approved the final manuscript as submitted and agree to be accountable for all aspects of the work.

## Additional Information

**Competing Interests:** The authors declare that they have no competing interests.

**Publisher's note:** Springer Nature remains neutral with regard to jurisdictional claims in published maps and institutional affiliations.



**Open Access** This article is licensed under a Creative Commons Attribution 4.0 International License, which permits use, sharing, adaptation, distribution and reproduction in any medium or format, as long as you give appropriate credit to the original author(s) and the source, provide a link to the Creative Commons license, and indicate if changes were made. The images or other third party material in this article are included in the article's Creative Commons license, unless indicated otherwise in a credit line to the material. If material is not included in the article's Creative Commons license and your intended use is not permitted by statutory regulation or exceeds the permitted use, you will need to obtain permission directly from the copyright holder. To view a copy of this license, visit <http://creativecommons.org/licenses/by/4.0/>.

© The Author(s) 2017